AD-A193 815 SQUID (SUPERCONDUCTING QUANTUM INTERFERENCE DEVICE) 1/1
ARRAYS FOR SIMULTANEO..(U) NEW YORK UNIV N Y
L KAUFMAN ET AL. 29 FEB 88 AFOSR-TR-88-0364
UNCLASSIFIED F49620-86-C-0131 F/G 20/3 NL

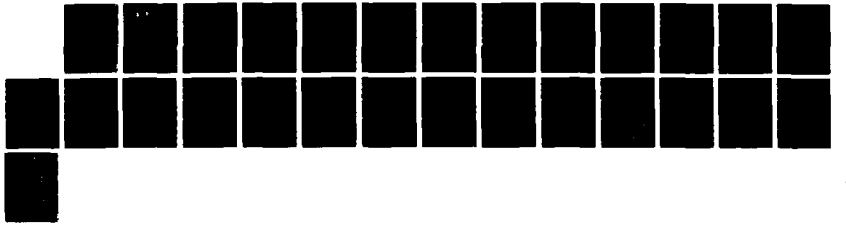

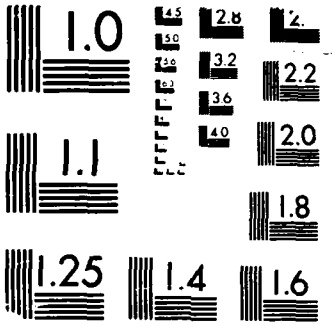

SECURITY CLASSIFICATION OF THIS PAGE

OCUMENTATION PAGE

Form Approved OMB No. 0704-0188

AD-A193 815

1b. RESTRICTIVE MARKINGS	
2b. DECLASSIFICATION / DOWNGRADING SCHEDULE	3. DISTRIBUTION / AVAILABILITY OF REPORT: Approved for public release distribution unlimited
4. PERFORMING ORGANIZATION REPORT NUMBER(S)	5. MONITORING ORGANIZATION REPORT NUMBER(S): AFOSR-TR- 88-0364
6a. NAME OF PERFORMING ORGANIZATION: New York University	6b. OFFICE SYMBOL (If applicable):
6c. ADDRESS (City, State, and ZIP Code): Departments of Psychology and Physics, 4 Washington Place - New York, NY 10003	7a. NAME OF MONITORING ORGANIZATION: Air Force Office of Scientific Research
8a. NAME OF FUNDING / SPONSORING ORGANIZATION: AFSOR	8b. OFFICE SYMBOL (If applicable): NL
8c. ADDRESS (City, State, and ZIP Code): Building 410, Bolling AFB, DC 20332	7b. ADDRESS (City, State, and ZIP Code): Building 410, Bolling AFB, DC 20332-6448
	9. PROCUREMENT INSTRUMENT IDENTIFICATION NUMBER: F49620-86-C-0131
	10. SOURCE OF FUNDING NUMBERS: PROGRAM ELEMENT NO. 61103D; PROJECT NO. 3484; TASK NO A4; WORK UNIT ACCESSION NO.

11. TITLE (Include Security Classification)
SQUID Arrays for Simultaneous Magnetic Measurements: Calibration & Source Localization Performance

12. PERSONAL AUTHOR(S)
Lloyd Kaufman, Samuel J. Williamson, and P. Costa Ribeiro

13a. TYPE OF REPORT	13b. TIME COVERED	14. DATE OF REPORT (Year, Month, Day)	15. PAGE COUNT
Publication	FROM Sept 86 TO Feb 88	Feb. 29, 1988	26

16. SUPPLEMENTARY NOTATION

17. COSATI CODES			18. SUBJECT TERMS (Continue on reverse if necessary and identify by block number)
FIELD	GROUP	SUB-GROUP	

19. ABSTRACT (Continue on reverse if necessary and identify by block number)

Recently developed small arrays of SQUID-based magnetic sensors can, if appropriately placed, locate the position of a confined biomagnetic source without moving the array. We present a technique with a relative accuracy of about 2% for calibrating such sensors having detection coils with the geometry of a second-order gradiometer. The effects of calibration error and magnetic noise on the accuracy of locating an equivalent current dipole source in the human brain are investigated for 5- and 7-sensor probes and for a pair of 7-sensor probes. With a noise level of 5% of peak signal, uncertainties of about 20% in source strength and depth for a 5-sensor probe are reduced to 8% for a pair of 7-sensor probes, and uncertainties of about 15 mm in lateral position are reduced to 1 mm, for the configuration considered.

20 DISTRIBUTION / AVAILABILITY OF ABSTRACT	21. ABSTRACT SECURITY CLASSIFICATION	
☐ UNCLASSIFIED/UNLIMITED ☒ SAME AS RPT ☐ DTIC USERS	unclassified	
22a. NAME OF RESPONSIBLE INDIVIDUAL: Dr. Alfred R. Fregly	22b. TELEPHONE (Include Area Code): 202-767-5024	22c. OFFICE SYMBOL: NL

DD Form 1473, JUN 86 — Previous editions are obsolete. — SECURITY CLASSIFICATION OF THIS PAGE

07 MAR 1988

To be published in:
IEEE Transactions in Biomedical Engineering

SQUID Arrays for Simultaneous Magnetic Measurements: Calibration and Source Localization Performance

P. COSTA RIBEIRO, S.J. WILLIAMSON, MEMBER, IEEE, AND L. KAUFMAN

Abstract - Recently developed small arrays of SQUID-based magnetic sensors can, if appropriately placed, locate the position of a confined biomagnetic source without moving the array. We present a technique with a relative accuracy of about 2% for calibrating such sensors having detection coils with the geometry of a second-order gradiometer. The effects of calibration error and magnetic noise on the accuracy of locating an equivalent current dipole source in the human brain are investigated for 5- and 7-sensor probes and for a pair of 7-sensor probes. With a noise level of 5% of peak signal, uncertainties of about 20% in source strength and depth for a 5-sensor probe are reduced to 8% for a pair of 7-sensor probes, and uncertainties of about 15 mm in lateral position are reduced to 1 mm, for the configuration considered.

This work was supported in part by AFOSR Grants F49620-85-K-0004 and F49620-86-C-0131

P. Costa Ribeiro was supported by the Guggenheim Foundation and is with the Departamento de Fisica, Pontificia Universidade Catolica do Rio de Janeiro, c.p. 38006, CEP 22453, Rio de Janeiro, Brazil.

S. J. Williamson and L. Kaufman are with the Neuromagnetism Laboratory, Departments of Physics and Psychology, respectively, New York University, New York, New York, 10003.

I. INTRODUCTION

Magnetic fields produced by biological activity provide important information concerning the location of electrical excitation in various organs, especially in the human brain for normal and abnormal functions.[1]-[5] The early success of neuromagnetism motivated the development of magnetic sensing systems to measure the magnetic field near the scalp at several positions simultaneously. Probes with 4, 5, and 7 sensors are presently in use.[6]-[9] In addition to greatly reducing the time required to record a field pattern, these multi-sensor systems make it possible to determine the position, strength, and orientation of a localized neural current source with a *single-position measurement*, that is, without having to move the probe from one place to another. A particular advantage of this is the possibility of following subtle shifts of activity between adjacent neural populations in studies such as those recording responses evoked by visual patterns of differing content.

A single-position measurement has major advantages as compared to serial measurements, since it avoids the complications that may be introduced by changes in the state of the brain, e.g., because of alterations in the subject's attention from one measurement to the next. Furthermore, a single-position measurement avoids inaccuracies in determining the relative sensor positions when a probe is moved from one position to another.

In this report we describe the requirements for successful single-position measurements with a small array of sensors. Among these requirements, the accuracy of the sensors' calibration is the most stringent. An erroneous calibration with a single-sensor system introduces only a systematic error in the strength of the source but not an erroneous source localization. However, when performing a single-position measurement with a multi-sensor system a discrepancy in calibration among the sensors will affect the deduced source location itself. A method is thus introduced for calibrating the individual sensors with the required high relative accuracy and rapidity. The effects of calibration errors and of magnetic and instrumental noise on the accuracy of localizing a current-dipole source are evaluated.

II. SENSOR CALIBRATION

Most biomagnetic sensors rely on the superconducting quantum interference device (SQUID) to achieve the high sensitivity required for measurements of the brain's magnetic field outside the body.[10] This provides an output voltage that varies linearly with the magnetic flux in a detection coil, which is magnetically coupled to the SQUID by means of a superconducting flux transformer. The detection coil generally has the geometry of a first-, second-, or third-order gradiometer with the baseline, or distance between adjacent coils, typically 4 to 8 cm. A gradiometer discriminates against ambient field noise sources that are relatively distant compared with the baseline because it suppresses the relatively uniform fields from distant noise sources while retaining sensitivity to the closer biomagnetic sources of interest, whose fields are much stronger at the closest coil.[10]-[12] This coil is often called the *pickup coil*.

Traditionally, to calibrate a single-coil detection coil (or *magnetometer*) a known, uniform field is imposed on the coil and the corresponding change in the sensor's output voltage is measured. However, this simple procedure cannot be used with gradiometers, since a well-constructed gradiometer will not respond to a uniform field. A common resolution to this problem is to apply the field by coaxially positioning a small field coil directly under the detection coil, pressing it firmly against the bottom of the cryogenic dewar containing the SQUID system and moving it until a maximum output from the SQUID is observed. From the dimensions of the field coil and detection coil, together with their relative positions, the mutual inductance of the coils can be computed. The product of the mutual inductance and the current in the field coil gives the magnetic flux imposed on the detection coil. It is conventional to express the field calibration factor K in terms of the field that must be applied to the pickup coil alone to produce the same output voltage from the SQUID sensor. This procedure, however, is inherently inaccurate because the various dimensions must be known to within a fraction of a millimeter. In practice the result has an accuracy of perhaps only 10%. A variation of this procedure relies on placing the coil in succession at a number of precisely determined locations sufficiently far from the probe that the field of the coil at the sensors is accurately dipolar. From the recorded outputs of all sensors for each coil location, high accuracy may be obtained when the calibration factors are determined by a least-squares fit.[13]

Sensitivity of the mutual inductance to the distance between field coil and detection coil is an intrinsic limitation of the calibration method due to the gradiometer itself. Indeed, another way to characterize a gradiometer as a spatial discriminator between the source of interest and distant sources of ambient field noise is through the reciprocity theorem.[14] According to that approach a system of coils (gradiometer) that is insensitive to far sources is also a system that if energized by a current will produce a field that decreases rapidly with increasing distance from the coils.[15] It is precisely this rapid variation of the field with distance that imposes the difficulty in calibrating a gradiometer. As an illustration, Leoni et al. show (Fig. 14 of [12]) that the flux imposed on a repesentative, symmetric, second-order gradiometer by a magnetic dipole varies inversely as the cube of the distance from the pickup coil until the dipole is approximately one baseline away, and beyond that varies more rapidly with distance. The decrease is less rapid for a first-order gradiometer, and Wikswo [16] has shown it is possible to calibrate such a detection coil with a field coil placed at various precisely determined distances from it along its axis. One feature of his technique is to use a solenoid for the field coil whose ratio of length to diameter is $(3/4)^{1/2}$, which has a dipole moment but no quadrupole moment.

A. Large-Coil Calibration Technique

We have successfully applied another method for calibrating second-order gradiometers that relies precisely on the fact that such coils are relatively insensitive to a uniform field. The procedure is to use a large, square field coil whose sides are roughly two orders of magnitude greater than the baseline of the detection coil. This *calibration coil* is placed so that the detection coil is coaxial and at its center. Letting the axial distance from the common center be denoted by z, the component of the field along this axis for a calibration coil of side $2S_c$ can be expanded in a power series of (z/S_c):

$$B_c(z) = [1 - (5/4)(z/S_c)^2 + (75/32)(z/S_c)^4 + \dots]\, B_c \quad (1)$$

where the field at the center of the coil is

$$B_c = \sqrt{2}\, \mu_o N_c I_c / \pi S_c \quad (2)$$

where N_c is the number of turns and I_c is the current in the coil.

It is conceptually helpful to think of the terms in Eq. 1 as the sum of separate components of the field that are superimposed on the detection coil. For purposes of illustration (Fig. 1) we consider a second-order gradiometer that has the center coil wound in the opposite sense with twice as many turns as the end coils. We suppose that all three coils have the same area A. Thus the uniform-field component of strength B_c produces no net magnetic flux in the detection coil if the sum of the area-turns products of these three coils is zero (perfect *field balance*). The term in Eq. 2 proportional to z^2 imposes a flux $-(5/4)(b/S_c)^2 B_c A$ in the pickup coil and other end coil but no flux in the center coil. The field calibration factor is determined by the field in the pickup coil alone that would produce the same total flux:

$$B_q = -(5/2)(b/S_c)^2\, B_c \quad (3)$$

We call this the *quadratic field component*. If the gradiometer's baseline b is small in comparison with the side $2S_c$ of the calibration coil, the fourth-order term in Eq. 1 is negligible compared with the quadratic term. Specifically, if $b = 0.04$ m and $S_c = 1.32$ m as in our apparatus, the fourth-order term is only 0.2% of the quadratic field.

1. Calibration Field Measurements

To calibrate our SQUID system,[1] our dewar containing the detection coils was

1. This commercial system (Biomagnetic Technologies, Inc., 4174 Sorrento Valley Blvd., San Diego, CA, 92121) has a set of five detection coils arranged in the pattern of a cross, with the outer coils tipped outward by 10° so their axes point to a common position 10.3 cm below their pickup coils. There are also four SQUID sensors positioned on the dewar's axis 8 cm above the center of the detection coils for the purpose of monitoring three orthogonal components of the ambient field and the axial field gradient (see Ref. 7). The attenuated output of these 4 reference sensors is electronically subtracted from each of the outputs of the 5 signal channels to reduce the effect of ambient field noise. However, during the procedures of gradiometer characterization and calibration described here these reference sensors are turned off, to minimize unwanted complications when interpreting the calibration results.

positioned so as to have the detection coil of interest centered coaxially within a square calibration coil of side $2S_c$ = 2.64 m and N_c = 57 turns. An ac current of amplitude I_c at 20 Hz was provided by a function generator, and the corresponding output of the SQUID electronics was amplified, bandpass filtered, and monitored by a digital voltmeter. With the amplitude of the uniform component set for $B_c = 8.00\times10^{-7}$ T, the quadratic field given by Eq. 3 is only $B_q = -1.84\times10^{-9}$ T. Each of the SQUID sensors in our 5-channel instrument yields a corresponding voltage output after amplification that is typically $V_c = -1.30\times10^{-2}$ V. Dividing B_q by this observed output voltage gives the desired calibration factor K in tesla/volt for the SQUID system. Of particular importance is the fact that this value is insensitive to the exact position of the calibration coil with respect to the detection coil: moving it upward or downward by 4 cm produces only a 1% change in the value of K. This is the desired feature of the large-coil technique.

The calibration factor determined in this way is accurate only to the extent that the field balance of the gradiometer is sufficiently good. Because B_q is only $-2\times10^{-3}B_c$, the field imbalance η must be smaller than 2×10^{-5} to be negligible in the presence of the uniform field B_c when 1% accuracy in the calibration factor is desired. In fact the imbalance in our detection coils is about $\eta = 2\times10^{-4}$, so it is essential to take field imbalance into account.

2. Uniform Field Measurements

The field imbalance for a gradiometer can be determined by applying a uniform field B_u and measuring the resulting output voltage of the sensor. For this purpose, a reasonably uniform field can be produced with a set of four coaxial, square coils [17] of side $2S_c$ = 2.64 m. Each of the inner coils was positioned at a distance $0.128{\cdot}2S_c$ from the center of the detection coil and each of the outer coils a distance $0.506{\cdot}2S_c$. The number of turns of wire in the four coils was originally 59, 25, 25, 59. These field coils were positioned with an accuracy of better than 2 mm in an attempt to achieve sufficient field uniformity. Theoretically the field at the center is given by:

$$B_u = 1.795\times10^{-6}\,(N_u I_u / 2S_c) \qquad (4)$$

where N_u = 59 is the number of turns in each outer coil and I_u is the current passing through the coils in series combination.

Precise measurements of the resulting axial field profile (in the vertical direction) were made to verify the quality of uniformity. This was done with a fluxgate magnetometer having two sensors so that it can be operated in a differential mode for increased sensitivity. One sensor was placed near the center of the field coils and the other, oriented in the opposite direction, was moved from one position to another along the axis. Unfortunately, these measurements revealed that the center of the field pattern was shifted upward by 5 cm from the geometrical center of the set of coils. We attributed this error to the effect of the magnetic susceptibility of steel reinforcing rods in the concrete floor of the laboratory (the lowest coil was only 5 cm above the floor) and corrected for the effect

by decreasing to 57 the number of turns of wire comprising the lowest coil. The center of the resulting field pattern then approximately coincided with the center of the coils, where the gradiometer was positioned. We denote this set of coils by the term *uniform-field coil.*

Measurements with the fluxgate magnetometer showed that the nonuniformity of the field pattern in the uniform-field coil produces a net flux of $1\times10^{-5}B_uA$ in the detection coil, corresponding to an equivalent field of $B_{nu} = 1\times10^{-5}B_u$ when related to the pickup coil. If the estimated field calibration factor for the SQUID were $K_e = 1\times10^{-7}$ T/V we would expect the corresponding output voltage from field nonuniformity to be $V_{nu} = B_{nu}/K_e = 1\times10^{-5}B_u/K_e = 7\times10^{-5}$ V for the current that we applied. This is much smaller than the field imbalance signal of the detection coil, as will now be described.

To measure the effect of field imbalance, a 20-Hz current was passed through the uniform-field coil, producing a field amplitude $B_u = 7.00\times10^{-7}$ T at its center. This is a convenient frequency for the calibration procedure, and its use is justified by the fact that we observed no frequency dependence in results obtained for lower frequencies. The corresponding ac output voltage V_u of each SQUID system was noted with a digital voltmeter. For our gradiometers, the typical output was $V_u = 2\times10^{-3}$ V, corresponding to $\eta = 3\times10^{-4}$. Of this only the amount $V_{nu} = 7\times10^{-5}$ V can be attributed to nonuniformity of the field, as was described in the preceding paragraph. The effect of nonuniformity is only 3.5% of the observed output voltage, thus justifying the use of an approximate field calibration factor in computing its contribution. To obtain the voltage V_{uf} expected for a truly uniform field, we must subtract from the observed voltage what is contributed by the nonuniformity: $V_{uf} = V_u - V_{nu} = 1.93\times10^{-3}$ V.

3. Computation of the Field Calibration Factor

Using the calibration coil we had observed that a typical SQUID system produced an output of $V_c = -1.3\times10^{-2}$ V. The desired part of this V_{cal} is due to the quadratic field component $B_q = -1.84\times10^{-9}$ T, and part is due to the field imbalance of the gradiometer in the uniform field $B_c = 8\times10^{-7}$ T. To deduce the latter voltage we need only scale V_{uf} by the ratio of the uniform fields B_c/B_u and subtract from the observed voltage:

$$V_{cal} = V_c - (B_c/B_u)V_{uf} \tag{5}$$

In our example the field imbalance correction is only about 15% of the observed voltage V_c, yielding $V_{cal} = -1.52\times10^{-2}$ V. The desired field calibration factor is then $K = B_q/V_{cal} = 1.21\times10^{-7}$ T/V.

In applying this procedure to a 5-sensor probe, we found that the value of the calibration factor K for each coil could be determined reproducibly with an accuracy of 2%. In comparing calibration factors K across coils we found a 10% spread in their values. This variability may be attributed to differences in the construction of the SQUID systems.

4. A Method of Verification

Another way to measure the field imbalance correction η, which at the same time verifies the value for the field calibration factor K, is to measure the change in the output when the calibration coil is moved axially up or down by a known distance. If the displacement is small it is enough to consider Eq. 1 only up to the fourth-order term. The change in the output voltage V_c for a displacement d from the detection coil's center will be:

$$\Delta V_c(d) = (B_c/K)\,[\,\eta - (5/2)(d/S_c)^2 + (225/8)(bd/S_c^2)^2\,] \qquad (6)$$

The two unknowns in this equation (η and K) can be determined with two measurements. When displacing the calibration coil in our system by 4 cm the output voltage changes by 1%, leading to the value $\eta = 2\times10^{-4}$.

For simplicity in the calibration procedure described here, one of the four large coils that produced the uniform field was used as the calibration coil. However, a smaller coil would make the calibration easier because the signal for a given displacement d is larger. One source of error in the calibration procedure is enhanced with a smaller calibration coil, but another source is diminished. First, with the calibration coil centered on the detection coil, the fourth-order term introduces an enhancement over that of the second-order term (Eq. 1) by the ratio

$$(75/32)(b/S_c)^4/(5/4)(b/S_c)^2 = 1.88\,(b/S)^2 \qquad (7)$$

Thus the output voltage must be corrected for this additional signal to obtain V_c. Second, the field imbalance η of the coil, in the presence of the uniform component of the field produces an error compared with the quadratic field of

$$\eta/(5/2)(b/S_c)^2 = 0.4\eta(S_c/b)^2 \qquad (8)$$

This decreases for smaller calibration coils. A good compromise would be to have both corrections (Eqs. 7 and 8) be equal in magnitude. For an imbalance of $\eta = 2\times10^{-4}$, this equality is attained with S = 49.5 cm, giving a total calibration error of +1.2% for the quadratic term and -1.2% for the field imbalance.

B. Single-Position Calibration

Another advantage of using a single large external coil for calibration is the possibility of doing it rapidly for all the sensors in an array. In fact it is not necessary to place each detection coil at the center and coaxially aligned with the calibration coil. The field

produced by a large square coil can be computed for the position of each turn of each detection coil. Provided that the diameter of each coil is negligible compared with that for the calibration coil, the flux within a gradiometer can be written as:

$$\Phi = \sum_{i=1}^{N} n_i B_i A \tag{9}$$

where n_i is the number of turns of each coil, N the number of coils in the gradiometer ($N = 3$ for a second-order gradiometer), B_i is the axial field at the coil's position, and A is the area of the coil. To compute the values of B_i it is useful to compute the three orthogonal components of the field B_{xjk}, B_{yjk}, B_{zjk} produced by a rectangular loop of wire lying at $x = \pm a$ and $y = \pm a$ and carrying a current I_c clockwise about the z-axis (Fig. 2). The distances of a field point at (x,y,z) in the positive octant from successive corners, starting with the nearest, are r_1, r_2, r_3, r_4, and the components of r_1 and r_3 are (x_1,y_1,z) and (x_3,y_3,z). Then the components of the magnetic induction in coil j of gradiometer k are:[18]

$$B_{xjk} = (\mu_o I_c/4\pi)\, z_{ik}\{[r_{1jk}(r_{1jk}-y_{1jk})]^{-1} + [r_{3jk}(r_{3jk}+y_{3jk})]^{-1} - [r_{4jk}(r_{4jk}+y_{3jk})]^{-1} - [r_{2jk}(r_{2jk}+x_{3jk})]^{-1}\}$$

$$B_{yjk} = (\mu_o I_c/4\pi)\, z_{jk}\{[r_{3jk}(r_{3jk}+x_{3jk})]^{-1} + [r_{1jk}(r_{1jk}-x_{1jk})]^{-1} - [r_{4jk}(r_{4jk}+x_{3jk})]^{-1} - [r_{2jk}(r_{2jk}+x_{3jk})]^{-1}\} \tag{10}$$

$$\begin{aligned} B_{zjk} = (\mu_o I_c/4\pi)\, \{ & x_{1jk}[r_{1jk}(r_{1jk}-y_{1jk})]^{-1} - [r_{4jk}(r_{4jk}+y_{3jk})]^{-1} \\ & + x_{3jk}[r_{3jk}(r_{2jk}-y_{1jk})]^{-1} - x_{3jk}[r_{3jk}(r_{3jk}+y_{3jk})]^{-1} \\ & + y_{1jk}[r_{1jk}(r_{1jk}-x_{1jk})]^{-1} - y_{1jk}[r_{2jk}(r_{2jk}+x_{3jk})]^{-1} \\ & + y_{3jk}[r_{4jk}(r_{4jk}-x_{1jk})]^{-1} - y_{3jk}[r_{3jk}(r_{3jk}+x_{3jk})]^{-1}\} \end{aligned}$$

In our case Eq. 9 can be written for each detection coil k as:

$$\Phi_k = 2A[\, \mathbf{B}_{-1k} - 2\mathbf{B}_{0k} + \mathbf{B}_{1k} \,] \cdot \mathbf{n}_k \tag{11}$$

where the coils j = -1, 0, 1 correspond to the pickup coil, middle coil, and upper coil respectively, and $\mathbf{n}_k$ is a unit vector pointing upward along the axis of detection coil k. Then Eq. 10 can be written more explicitly in matrix notation as:

$$\Phi_k = 2A\{(B_{x\text{-}1k} - 2B_{x0k} + B_{x1k}) \quad (B_{y\text{-}ik} - 2B_{y0k} + B_{yik}) \quad (B_{z\text{-}ik} - 2B_{z0k} + B_{zik})\} \begin{Bmatrix} n_{xk} \\ n_{yk} \\ n_{zk} \end{Bmatrix} \tag{12}$$

For our 5-sensor system there are 5 of the $\mathbf{n}_k$ 1×3 matrices, one for each detection coil, as determined by the geometrical configuration of the array (as an example, see the Appendix for their values for the present system). There are also 15 values of the type B_{xjk}, three for each detection coil to be evaluated using Eq. 9. In order to compute them we need to know $r_1, r_2, r_3, r_4, x_1, y_1, x_3, y_3$, and z for each coil j of each detection coil k. The total flux will then vary among detection coils, as given by the expression:

$$\Phi_k = 2A\,(\mu_o I_c / 4\pi) f_k \tag{13}$$

The f_k factors describe the sensor array and depend on its particular geometric configuration. In our system, as described earlier, there is one central detection coil, with 4 others equally-spaced about it. In this case, with the central coil upright and centered in the calibration coil, f_k is found to differ by 10% between the central coil and any one of the outer ones.

Although this calibration procedure is comparatively insensitive to the vertical position of the calibration coil, it is nevertheless sensitive to other parameters such as the size of that coil: a 1% change in the length of the sides of the calibration coil affects the calibration by 3%. On the other hand, an error in the angular orientation by 1 deg affects the calibration by only 0.16%.

Another advantage of this single-position calibration, beyond its rapidity, is the possibility of using it to determine the exact angular position of the array relative to a fixed laboratory frame of reference (the calibration coil) during an experiment where the array is tipped in order to be positioned over the source. The calibration factors f_k can be determined prior to such a measurement, with the array upright, by passing a known current through the calibration coil.

III. Influence of Calibration Errors on Locating a Source

In the preceding section we presented a method for accurately calibrating each detection coil in a multi-sensor system. Now we explain why such accurate calibration is needed by considering how calibration errors affect the accuracy in locating a biomagnetic source. For purposes of illustration, we shall take the example of a localized region of active neurons in the human brain, which may be modeled by an equivalent current dipole. This model is appropriate when the largest linear extent of the active neural volume is much smaller than the distance to the detection coil. The current dipole Q is simply a vector representing a short line element of current. Its magnitude Q is the product of the current and the length of its extent and correspondingly has the dimensions of ampere-meter. In the present context, the observed current dipole represents the vector sum of individual current dipoles for each contributing neuron. To interpret scalp potentials or magnetic field patterns, it is common to model the head as a uniform sphere or a set of concentric spherical shells of differing conductivity, representing regions such as the brain, skull, and dermis. Then only the component of the current dipole tangential to the surface is detected magnetically, and the field pattern outside the head is independent of the radial variation of conductivity. Thus the current dipole is described by five parameters: its position (x, y, z), orientation ψ of its moment in the tangent plane, and the value Q of this moment.

The five field values obtained from a single-position measurement with a 5-sensor probe are sufficient to determine these five parameters, provided that the probe is not centered on certain symmetry lines or points (such as directly over the dipole).[19,20] Indeed, if additional information is available to fix the orientation of the source, a four-sensor system may serve for locating a dipole.[21] However, we might expect that locating a dipole with a 4- or 5-sensor system is very sensitive to calibration errors since the parameters are not overdetermined by the data. In addition to assessing this, we shall examine how the uncertainty in parameter values due to noise is reduced for successively larger arrays of sensors presently in use: a 5-sensor probe with 4 outer coils equally spaced about a central coil; a 7-sensor probe with 6 outer coils equally spaced about a central coil; and a pair of 7-sensor probes (hereafter called a 14-sensor system).

The probe in these computations will be placed directly over a position on the scalp where the normal component of the field is maximum, which is useful for achieving good accuracy in determining the depth and strength of a current dipole. It should be borne in mind that such a strategy is not optimal for all purposes, for example in determining the dipole's position longitudinal and transverse to the direction of its moment. Greater precision may be gained in transverse position with a single probe by placing it closer to the dipole where the field changes most rapidly with lateral position; however, at the same time, precision is sacrificed for the determination of some other parameters. As our primary purpose is to give an indication of how source localization is improved by larger numbers of sensors, we need not consider all possible arrangements of the probes.

A. Field Pattern of a Current Dipole

Figure 3a illustrates a 5-sensor probe positioned over the positive field extremum of a current dipole in a spherical head. The dipole lies at coordinates ($x = 0$, $z = 0$) of a Cartesian system centered in the head, at a depth $d = 2$ cm beneath the surface of the head of radius 9 cm. It has a moment of magnitude $Q = 1$ nA·m, which is oriented in the y-z plane, parallel to the $+z$ direction. This orientation is defined as $\psi = 0^{\circ}$. The flux in each detection coil is equivalent to having the following field in the respective pickup coils: for Sensor 1: 21.93 femtotesla; for 2 and 4: 16.27 fT; for 3: 16.15 fT; and for 5: 7.98 fT.

In the following discussion it is helpful to keep in mind that the distance between the two field extrema, in comparison with the radius of the head, fixes the depth of the dipole. The deduced depth increases with the ratio of these lengths.[22] Similarly, the spatial frequency spectrum describing the variation of field near an extremum shifts toward longer wavelengths with increasing depth; hence, the ratio of the field at the center sensor (Sensor 1) to the field at any outer sensor decreases with increase in depth.

B. Multi-Sensor Probes

1. Five-Sensor Probe

The probe we consider has a set of five detection coils, each being a second-order gradiometer with a coil radius $a = 0.75$ cm and baseline $b = 4.0$ cm between adjacent coils. The coils are arranged in the pattern of a cross (Fig. 3a), so that the centers of the pickup coils of the four outer coils are 2.0 cm from the axis of symmetry. The pickup coil of each gradiometer is positioned above the surface of the head by 1.3 cm (representing the thickness of the dewar containing the probe). The axes of the outer coils are tipped outward at the top by an angle of 10°, so that they point to a common position on the axis about 10.3 cm beneath the central pickup coil, coinciding with the center of the head. Consequently, the detection coils respond only to the radial component of the magnetic field of the dipole.

2. Seven-Sensor Probe

This probe is identical to the 5-sensor probe except that it has two additional outer sensors, thus forming a hexagonal array about the center coil (numbered sensors in Fig. 3b).

3. Fourteen-Sensor Probe

This consists of two 7-sensor probes, positioned at each field extremum with identical orientations (full set of sensors in Fig. 3b).

C. Effect of Calibration Errors

Certain detection coil positions play more important roles than others in determining the values of various dipole parameters obtained from a least-squares fit to the data. To illustrate this we have computed the consequence of a calibration error in any one of the sensors. The effect of a given percentage error for the calibration factor K of a sensor was computed by incrementing the value of its field and starting a least-squares fitting program with the actual dipole parameters as the initial condition. Nonlinearity in the relationship between field values and best-fitting parameters was evident, because identical positive and negative increments generally changed each parameter in opposite directions but by different amounts. We take the larger change to characterize the corresponding uncertainty in the best-fitting value. Figure 4 characterizes this maximum percentage change for errors ranging up to 14% in each of the 5 sensors. Our computations show that an error as small as 1% in *any* sensor causes the dipole to rotate and shift by ~5 mm in the coordinate z longitudinal to the direction of the dipole. This is indicated in Fig. 4 by the horizontal lines near the origin. If the errant sensor lies off the axis passing through the extrema of the field pattern (sensors 2 and 4), the shift is due to breaking of mirror symmetry about this line. If the errant sensor lies on the axis, there is no appreciable shift for negative errors in the value of K, but for positive errors there are two best-fitting solutions lying symmetrically on either side of the axis.

The lateral position x is influenced most strongly by errors in the center sensor and the one farthest from the dipole. The center field in comparison with fields at the outer sensors fixes the depth of the dipole and therefore how far it lies from the probe. Longitudinal position z is also influenced more strongly by coils lying farther from the dipole. The orientation ψ of the dipole's moment is related to this, being most sensitive to error in the farthest sensor, with all of the others being much less important.

Figure 4 also shows that the deduced depth d of the dipole is most sensitive to a calibration error for the center sensor. This is because its signal in comparison with those of the outer sensors determines the scale length of the pattern: a stronger signal decreases the length scale, thus implying a shallower dipole, and *vice versa*. The strength Q of the dipole is also most sensitive to the field indicated by the center sensor. While Q is directly related to the field at the extremum it is also affected by the depth of the dipole: to produce a given maximum field, the deduced Q must increase with increasing depth.

Similar computations have been carried out for 7-sensor and 14-sensor probes. The effects of calibration errors for the center sensor, sensors nearest the dipole, or sensors farthest from the dipole are similar, but the magnitude of the maximum shift of a dipole parameter is generally reduced. Part of this advantage comes from the effect of diluting the importance of any one sensor when the total number of sensors is increased, and in the case of the 14-sensor probe part comes the broader expanse of the field pattern that is sampled. One exception to the improvement in accuracy with increasing number of sensors is determination of the parameters Q and d with the 5-sensor and 7-sensor probes. This is because the center sensor has dominant importance for these parameters in comparison with any of the outer sensors, so a calibration error for the center sensor produces

virtually the same change in Q and d for both the 5-sensor and 7-sensor probes. To emphasize this point, there is a dramatic improvement in the precision for Q and d when the second 7-sensor probe is positioned over the other field extremum to produce a 14-sensor system. Determining the locations of the two extrema fixes the length scale of the pattern more firmly than the ratio of central to outer fields of any one extrema, thus reducing the importance of both center sensors.

These trends indicate that the scalar properties (strength Q and depth d) have values that are most sensitive to calibration errors in the central sensor, whereas the vector properties (longitudinal and transverse position, as well as orientation) are most sensitive to the coils placed farthest from the source. We emphasize that these trends apply when the probes are placed directly over the field extrema, so as to monitor the strongest fields. There is no implication in this choice of position that it is optimal for determining the full set of dipole parameters; indeed, the optimal position and orientation of the probe will depend on the parameter of interest and on the depth of the dipole.

IV. Influence of Noise on Locating a Source

The preceding discussion of calibration errors has a straightforward extension to the effect of field noise on the uncertainty in the best-fitting values of the dipole parameters. When a weak noise field δB_i is superimposed on the dipole's field in the i'th detection coil of an N-sensor probe, the corresponding change δP^j in the j'th parameter can be expressed as:

$$\delta P^j = \sum_{i=1}^{N} M_{ji}\, \delta B_i \tag{14}$$

where $M_{ji} = \partial P^j / \partial B_i$. For simplicity we assume that the noise in the various sensors is uncorrelated and of the same rms value δB_{rms}. Then the corresponding rms uncertainty in P^j is:

$$\delta P^j_{rms} = \left[\sum_{i=1}^{N} M_{ji}^2 \right] \delta B_{rms} \tag{15}$$

While this is a simple expression, inspection of Fig. 4 for the 5-sensor probe shows that some of the dipole parameters are not linearly related to changes in the field indicated by various sensors. Nevertheless, we shall use the linear approximation since our principal concerned is to obtain an estimate of how the uncertainty in parameter values is affected by the number of sensors. Thus in estimating the rms uncertainty for typical noise levels of 5% and 10%, we approximate the curves of Fig. 4 by straight lines through the

parameter values at the indicated noise value. Curves similar to those of Fig. 4 for the 7-sensor and 14-sensor probes show improved linearity. Recall that the values in Fig. 4 are based on the *maximum* error for either positive or negative deviations from the correct calibraton, so our procedure will tend to overestimate the corresponding effect of noise on parameter values.

To generalize the discussion, it is convenient to express the rms field noise in any sensor in terms of the field at the positive extremum $\delta B_{rms}/B_1$. Thus, when the same normalized noise amplitude is applied to an outer coil, which has a lower signal level, the actual signal-to-noise ratio for that coil is worse than for the center coil. The results for the 5-sensor, 7-sensor, and 14-sensor probes are shown in Table I. On going from 5 to 7 sensors, there is substantial improvement in reducing the uncertainties for some parameters (x, z, ψ), while there is very little benefit for others (Q and d). The most dramatic improvement is obtained on going from the 7-sensor to 14-sensor probe, where all the uncertainties are diminished. The reason is evident: On going from 5 to 7 sensors the additional outer detection coils enhance the probe's ability to resolve asymmetry in the field pattern, and this better establishes the position (x,z) and orientation ψ of the source with respect to a field extremum. A similar improvement is seen on going from 7 sensors to 14 sensors, but there is also a marked improvement in determining Q and d. The latter benefit was gained because placing a second probe over the second field extremum accurately fixes the distance between the extrema of the pattern, thereby more accurately determining d. Then the average of the field values accurately fixes Q. In addition, determining the general location of both extrema limits the uncertainty in the dipole's orientation ψ. This was said in a different way by Ahonen et al. [23] who noted that the accuracy of a dipole fit is enhanced for an array of sensors if the lateral spacing between their detection coils is increased, even if the dipole lies at a relatively shallow depth.

Cuffin [24] has also considered the effect of noise on dipole localization for several types of measurements, e.g., a large number of positions across a grid over the head, a 5-sensor probe of the kind we have considered, a 9-sensor probe (our 7-sensor probe but with two additional outer sensors), and a 5-sensor probe with three additional measurements from single-sensor probes at positions comparatively far from the source. Using a least-squares fitting procedure, he determined the dipole parameters for data with a Gaussian distribution of noise. One difference between his computations and ours is that the probe was not centered exactly on a field extremum but slightly to the side of it. Nevertheless, with 5% noise, there is general agreement between his results and ours for the uncertainty in strength, orientation, and depth of the dipole source. However, our uncertainty for the lateral position is about twice that of Cuffin's for the 5-sensor probe, while being less than his for our 7-sensor probe as compared with his 9-sensor probe. Uncertainties are dramatically reduced when data from remote measuring positions are included, with our 14-sensor determination having uncertainties that are about half of his for a 5-sensor probe augmented by 3 additional measurement positions.

The trends in Table I are the most important features to consider, not the exact values. This is because in actual measurements it is unlikely that a probe will be placed precisely as we have chosen. Furthermore, we have considered a dipole whose depth is relatively shallow and comparable to the lateral spacing between detection coils. A

depth much greater than this spacing will increase the parameter uncertainties since the greater spread of the field pattern produces a smaller percentage difference among fields applied to the detection coils. With this in mind, it may be concluded that the 5-sensor probe with a 10% noise level produces rather poor results: the source strength is known to only about 40%, its orientation to only 60°, and the lateral position to only 2 cm. Decreasing the noise to 5% provides substantial improvements, with uncertainties that are comparable to much of the data being reported in the literature with a single sensor being used for sequential measurements at some 30 or more positions.

The main advantage in adding two more sensors to produce a 7-sensor probe is in improving the uncertainty in position and orientation of the dipole. For a comparable noise level, these uncertainties are reduced by a factor of 2 - 3. A further reduction of ~3 is achieved in the uncertainties for *all* parameters by going to a 14-sensor probe. Here the results are comparable to what might be considered state-of-the-art, where Q and d are known to about 10%, transverse position to 1-2 mm, and orientation to 10°. Clearly, a 5% noise level with a 14-sensor probe would represent a substantial advance on this. High precision of this type is advantageous when searching for subtle changes in position or orientation of a confined neural population under study.

V. Conclusions

The computations described above demonstrate the importance of having an accurate relative calibration of individual sensors that are operated as a fixed array for determining the position, depth, orientation, and strength of a current dipole source. We have described techniques based on using a calibration coil of large size that can provide a calibration accuracy of 2% by a straight-forward procedure. Assuming such accuracy is attained, we investigated the limiting effects of noise on the precision with which dipole parameters can be established. When a 5-sensor probe is placed where it monitors the strongest signal, directly over a field extremum, then in the presence of 5% noise we expect to have uncertainties of about 20% for the source strength and depth. In addition there will be uncertainties in position of about 15 mm longitudinal to the dipole's direction and 5 mm in the transverse direction. Increasing the number of sensors to 7 leaves the former unaffected while reducing the position uncertainties by a factor of 3. Using two 7-sensor probes placed over the extrema reduces the uncertainty in strength and depth to less than 8% and in lateral position to less than 1 mm. These small uncertainties are comparable to the practical limits imposed by variability of many types of biomagnetic activity and by errors attendant to positioning a probe over the scalp.

Acknowledgements

We thank Dr. Carley Paulsen, Dr. Risto Ilmoniemi, and Bruce Luber for helpful discussions and assistance with the calibration measurements.

TABLE I

Magnitude of the uncertainties in best-fitting current-dipole parameters for various levels of field noise in the sensors. Noise is expressed as a percentage of the dipole's field at a field extremum. The dipole is located at a depth of 2 cm beneath the surface of a uniform conducting sphere of radius 9 cm.

PROBE (%)	NOISE (%)	$\delta Q/Q$ (%)	$\delta d/d$ (%)	δx (mm)	δz (mm)	$\delta \psi$ (deg)
5-sensor	5	21	16	4.6	13.6	40
	10	42	31	6.7	20.0	64
7-sensor	5	20	15	1.2	4.0	12
	10	44	31	2.6	8.1	14
14-sensor	5	8	6	0.4	1.0	3
	10	16	11	0.8	1.9	6

APPENDIX

This appendix illustrates how to specify the probe geometry for a single-position calibration of a multi-sensor SQUID system when using a square field coil, as described in Eqs. 10 - 12. We specify a 5-sensor SQUID system, as described in the text, when the middle of the central detection coil coincides with the center of a square field coil of side $2S = 2.64$ m. The orientations of the individual detection coils k are described by the elements of the unit vectors $\mathbf{n}_k = (n_{xk}, n_{yk}, n_{zk})$ given in the table, with z corresponding to the direction of the field coil's axis, which coincides with the axis of the central detection coil labeled $k = 1$.

Components of the orientation vectors $\mathbf{n}_k$

for the 5-sensor probe

Detection coil k	n_{kx}	n_{ky}	n_{kz}
1	0	0	1.000
2	0.174	0	0.985
3	0	0.174	0.985
4	-0.174	0	0.985
5	0	-0.174	0.985

Distances between the i'th corner of the field coil and the j'th coil of detection coil k are denoted by r_{ijk}. The components along the sides of the field coil of the corresponding vector of length r_{ijk} are denoted by (x_{ijk},y_{ijk},z). The last table illustrates these values for detection coil $k = 2$.

Relevant distances between the field coil and detection coil $k = 2$

Coil j	r_{1j2} (cm)	r_{2j2} (cm)	r_{3j2} (cm)	r_{4j2} (cm)	x_{1j2} (cm)	y_{1j2} (cm)	x_{3j2} (cm)	y_{3j2} (cm)	z (cm)
-1	185.44	188.01	188.01	185.44	130.18	132.00	133.82	132.00	4.16
0	184.90	188.47	188.47	184.90	129.48	132.00	134.52	132.00	0.22
1	184.46	189.00	189.00	184.46	128.79	132.00	135.21	132.00	3.72

REFERENCES

[1] S.J. Williamson, G.L. Romani, L. Kaufman, and I. Modena, Eds., *Biomagnetism: An Interdisciplinary Approach*, New York: Plenum, 1983.

[2] R. Hari and R.J. Ilmoniemi, "Cerebral magnetic fields," *CRC Critical Reviews on Biomed. Eng.*, vol. 14, pp. 93-126, 1986.

[3] S.J. Williamson and L. Kaufman, "Analysis of neuromagnetic signals" in *Handbook of Electroencephalography and Clinical Neurophysiology, Revised Series*, vol. 1, A. Gevins and A. Rémond, Eds., Amsterdam: Elsevier, pp. 405 - 448, 1987.

[4] R. Ricci, R. Leoni, G.L. Romani, F. Campitelli, S. Buonomo, and I. Modena, "3-D neuromagnetic localization of sources of interictal activity in cases of focal epilepsy", in *Biomagnetism: Applications and Theory*, H. Weinberg, G. Stroink, and T. Katila, Eds., New York: Pergamon, pp. 304-315, 1985.

[5] D.S. Barth, W. Sutherling, and J. Beatty, "Fast and slow magnetic phenomena focal epileptic seizures," *Science*, vol. 226, 855-857, 1984.

[6] R.J. Ilmoniemi, R. Hari, and K. Reinikainen, "A four-channel SQUID magnetometer for brain research," *Electroenceph. Clin. Neurophysiol.*, vol. 58, 467-473, 1984.

[7] S.J. Williamson, M. Pelizzone, Y. Okada, L. Kaufman, D.B. Crum, and J.R. Marsden, in *Proceedings of the Tenth International Cryogenic Engineering Conference*, H. Collan, P. Berglund, and M. Krusius, Eds., Guildford: Butterworth, pp. 339-348, 1984.

[8] G.L. Romani, "Multichannel instrumentation for biomagnetism," in *SQUID '85: Superconducting Quantum Interference Devices and Their Applicatons*, H.D. Hahlbohm and H. Lübbig, Eds., Berlin: Walter de Gruyter, pp. 919-932, 1985.

[9] J. Clarke, "Superconducting quantum interference devices for low frequency measurements," in *Superconducting Applications: SQUID's and Machines*, B.B. Schwartz and S. Foner, Eds., New York: Plenum, pp. 67-124, 1977; "Advances in SQUID Magnetometers," *IEEE Trans. Elec. Dev.*, vol. ED-27, pp. 1896-1908, 1980; "Fundamental limits on SQUID technology", in *Advances in Superconductivity*, B. Deaver and J. Ruvalds, Eds., New York: Plenum, pp. 13-50, 1983.

[10] J.E. Zimmerman, "SQUID instruments and shielding for low-level magnetic measurements," *J. Appl. Phys.*, vol. 48, pp. 702-710, 1977.

[11] J.P. Wikswo, Jr., "Optimization of SQUID differential magnetometers," *American Institute of Physics Conference Proceedings*. vol. 44, pp. 145-149, 1978.

[12] G.L. Romani, S.J. Williamson, and L. Kaufman, "Biomagnetic Instrumentation," *Rev. Sci. Instrum.*, vol. 53, pp. 1815-1845, 1982.

[13] R.J. Ilmoniemi, personal communication.

[14] For a discussion of the reciprocity theorm, or lead-field theory, see J.H. Tripp, "Physical Concepts and Mathematical Models" in *Biomagnetism: An Interdisciplinary Approach*, S.J. Williamson, G.L. Romani, L. Kaufman, and I. Modena, Eds., New York: Plenum Press, pp. 101-139, 1983.

[15] J.R. Storey, "Magnetic sensors with good signal-to-noise interference discrimination", *Il Nuovo Cimento*, vol. 2D, pp. 153-165, 1983.

[16] J.P. Wikswo, Jr., *Non-Invasive Magnetic Measurements of the Electrical and Mechanical Activity of the Heart*, Ph.D. Thesis, Department of Physics, Stanford University, pp. 128-135, 1975.

[17] R. Merritt, C. Purcell, and G. Stroink, "Uniform magnetic field produced by three, four, and five square coils," *Rev. Sci. Instrum.*, vol. 54, pp. 879-882, 1983.

[18] *American Institute of Physics Handbook*, 3rd Edition, McGraw Hill, New York, pp. 5-28, 1972.

[19] M.S. Hämäläinen, R.J. Ilmoniemi, J. Knutila, and K. Reinikainen, "Analysis of magnetoencephalographic data obtained with a four-channel SQUID magnetometer," in *Biomagnetism: Applications and Theory*, H. Weinberg, G. Stroink, and T. Katila, Eds., Oxford: Pergamon Press, pp. 299-303, 1985.

[20] R.J. Ilmoniemi, "Use of multisensor SQUID systems in brain research," in *SQUID '85: Superconducting Quantum Interference Devices*, H.D. Hahlbohm and H. Lübbig, Eds., Berlin: Walter de Gruyter, pp. 909-917, 1985.

[21] V.L. Vvedensky, R.J. Ilmoniemi, and M.J. Kajola, "Study of the alpha rhythm with a 4-channel SQUID magnetometer," Med. and Bio. Eng. and Comput. 23 Suppl., Part 1, 11-12, 1985.

[22] S.J. Williamson and L. Kaufman, "Evoked cortical magnetic fields," in *Biomagnetism*, S.N. Erné, H.D. Hahlbohm, and H. Lübbig, Eds., Berlin: Walter de Gruyter, pp. 353-402, 1981.

[23] A.I. Ahonen, J.K. Hällström, M.J. Kajola, J.E. Knuutila, C.D. Tesche, and V.A. Vilkman, "Design of a 7-channel dc-SQUID gradiometer for brain research", in *Proceedings of the Eleventh International Cryogenic Engineering Conference*, 1986.

[24] B.N. Cuffin, "Effects of Measurement Errors and Noise on MEG Moving Dipole Inverse Solutions", *IEEE Trans. Biomed. Eng.*, vol. BME-33, pp. 854-861, 1986.

FIGURE CAPTIONS

Fig. 1. Second-order gradiometer (a) with radius a and baseline b alongside a graph (b) showing the axial variation of the axial field applied by a single large coil, together with the uniform and quadratic components.

Fig. 2. Geometry for computing the field from a square calibration coil.

Fig. 3. a) A 5-sensor probe centered on the positive field extremum of a current dipole Q lying on the y-axis and directed along the z-axis. Curves qualitatively denote isofield contours. b) A 7-sensor probe (numbered sensors) or pair of 7-sensor probes (all sensors) positioned over the field extrema of the same dipole.

Fig. 4. Magnitude of the change in a dipole's best-fitting parameters arising from an error in the calibration factor K for each sensor of a 5-sensor probe centered on the positive field extremum (Fig. 3a). A curve describing more than one sensor is indicated by superimposed symbols for the respective sensors. The maximum change in each parameter is indicated when the calibration factor of the i'th sensor is incremented by the percentage given on the abscissa. Note that values for $\delta Q/Q$, $\delta d/d$, δz, and δy are reduced by a factor of 10 to fit onto the scale.

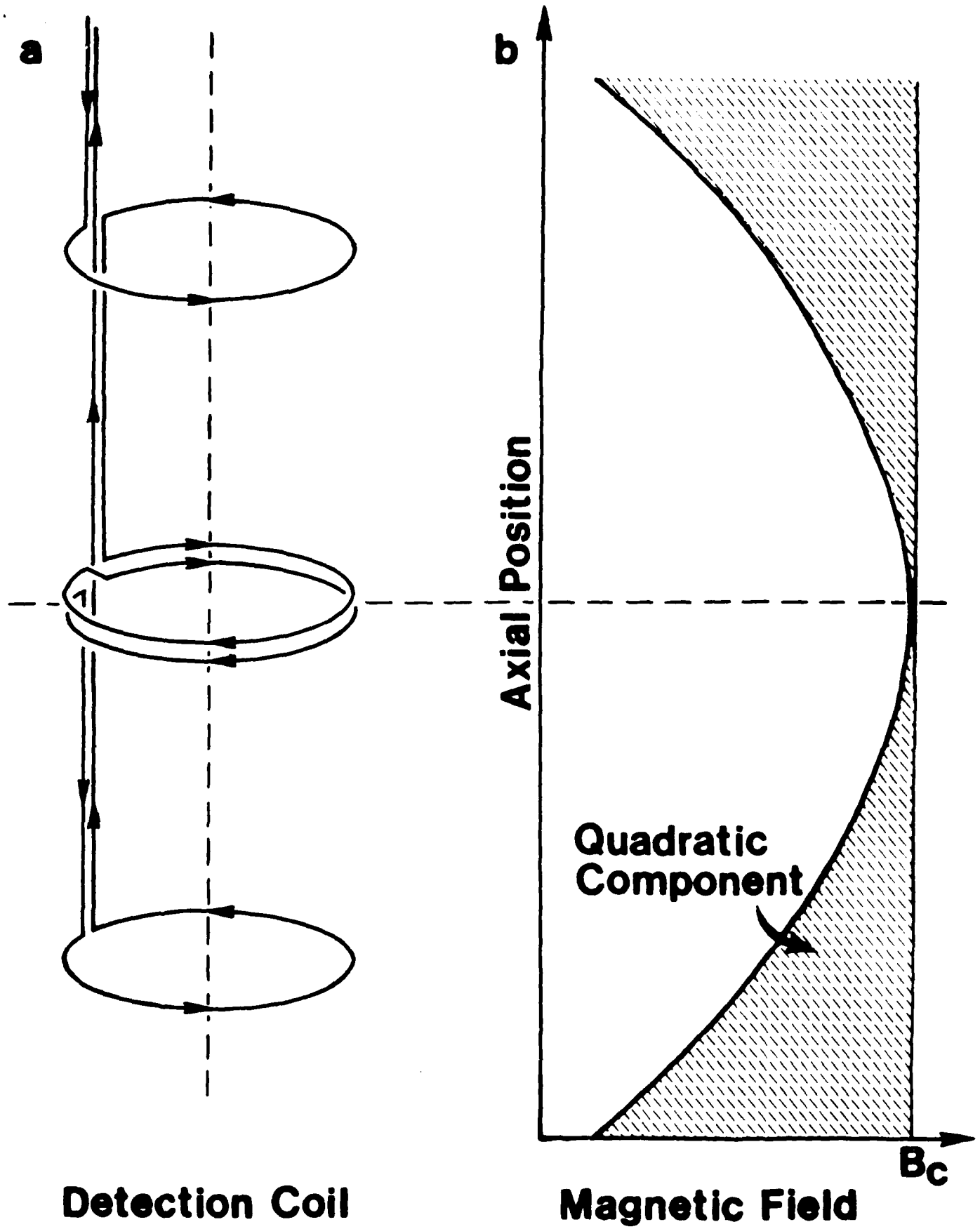
a
b
Axial Position
Quadratic
Component
B_C
Detection Coil
Magnetic Field

FIGURE 1

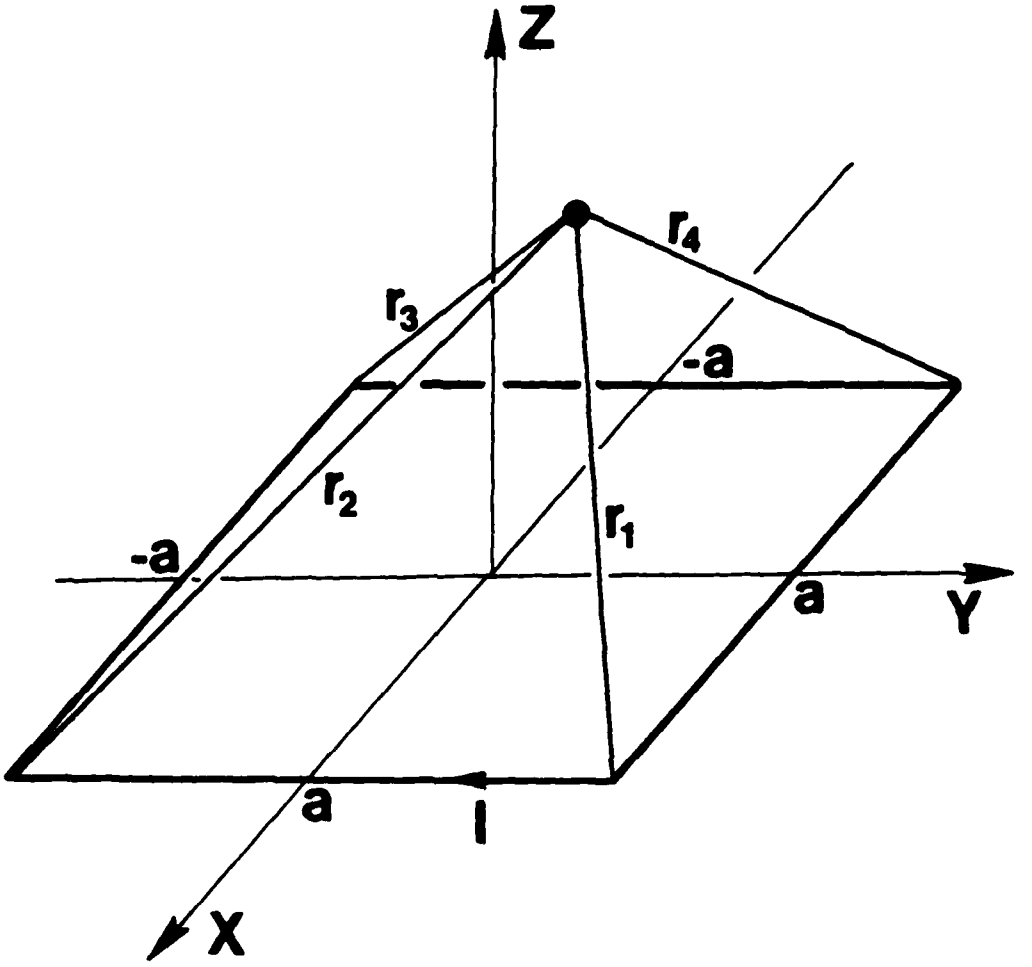

FIGURE 2

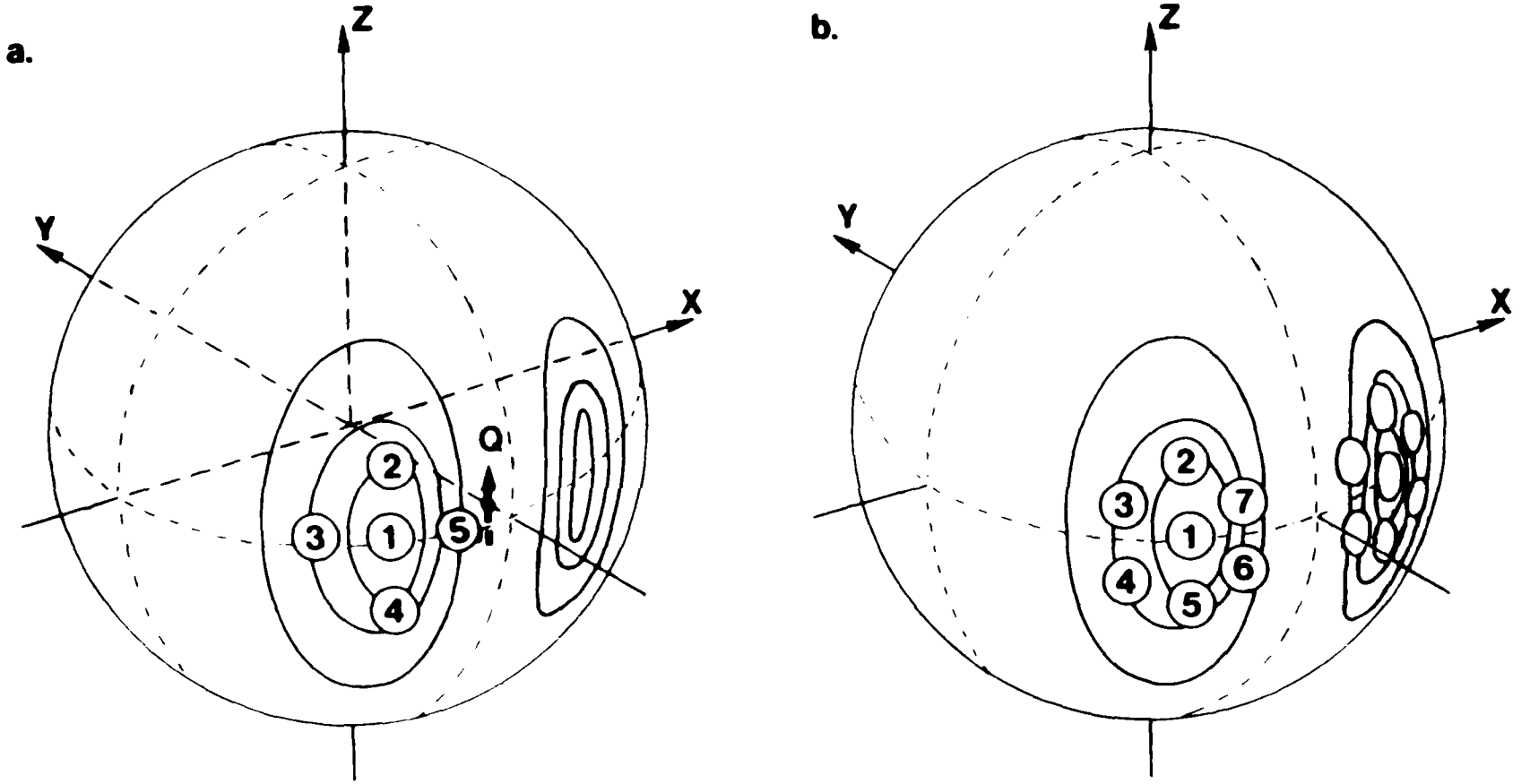

FIGURE 3

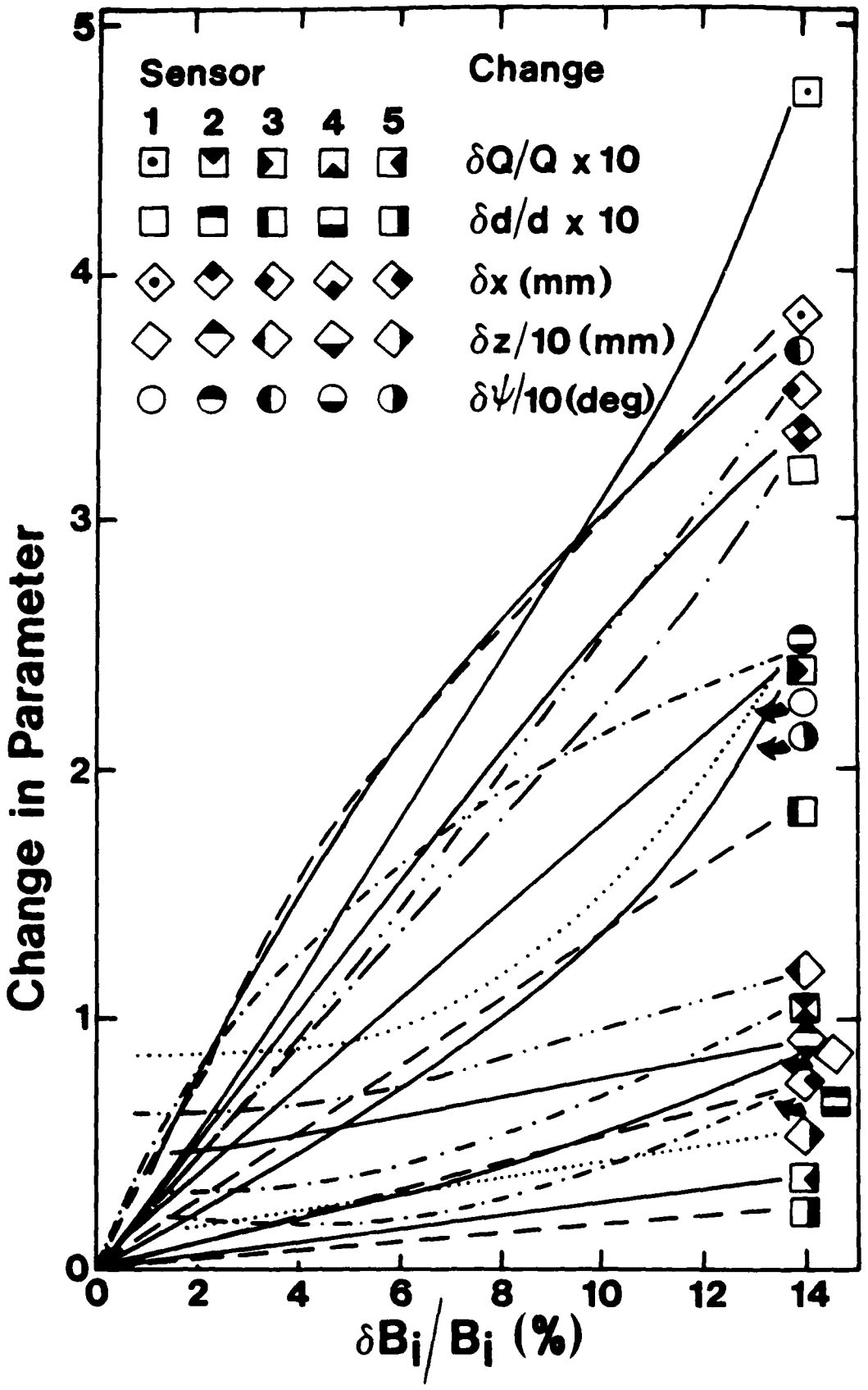
Sensor
Change
1 2 3 4 5
δQ/Q x 10
δd/d x 10
δx (mm)
δz/10 (mm)
δψ/10(deg)
Change in Parameter
0
1
2
3
4
5
0 2 4 6 8 10 12 14
δBi/Bi (%)

FIGURE 4

END

DATE

FILMED

8-88

DTIC